

Vision Guided Multi-Probe Assembly of 3D Microstructures

John D. Wason, John T. Wen

Center for Automation Technologies & Systems
Rensselaer Polytechnic Institute
Troy, NY 12180
{wasonj,wenj}@rpi.edu

Young-Man Choi, Jason J. Gorman, Nicholas G. Dagalakis

Intelligent Systems Division
National Institute of Standards and Technology
Gaithersburg, Maryland 20899-8230
{young-man.choi,jgorman,nicholas.dagalakis}@nist.gov

Abstract—This paper describes the operator assisted automated assembly of a 3-legged spatial platform by using a vision guided multi-probe assembly process. This is the first step towards the ultimate goal of building a microscale active spatial platform. Two issues are highlighted in this paper: contact management and vision feedback. Using multiple probes for part grasping and manipulation has the advantage of robustness and versatility as compared to micro-grippers. However, the contacts between the probes and the part need to be carefully managed to ensure a grasp that is stable for part pick-up and yet manipulable to allow part motion in a controlled fashion. By using vision guidance, the probes can be coordinated to grasp the parts and lift them off the die securely and reliably. We show that the contacts act as point contacts with friction, so when a part is pressed against a stationary probe, the part rotates about the axis between the contacts, changing its orientation so it may be inserted into a slot in the substrate. We have demonstrated that the three legs can be assembled in a fully automated fashion via multiple-camera vision feedback. The platform is at present assembled via tele-operation. The assembled microstructure measures $450\ \mu\text{m} \times 600\ \mu\text{m}$. We are now working on the full automation of the assembly onto a substrate populated with MEMS actuators.

I. INTRODUCTION

Assembly of microscale structures has been the focus of significant studies in recent years [1]–[12]. Numerous concepts have been proposed to move beyond planar Microelectro-mechanical system (MEMS) devices to spatial mechanisms through the assembly of parts manufactured using bulk micromachining processes. These efforts have produced functional spatial structures that would be difficult if not impossible to fabricate using the traditional photoresist-etch procedures. However, they are passive structures that are either fixed to the substrate, or mounted on a moving component that has been bulk micromachined.

Motivated by the planar actuated platform developed at NIST [13] as shown in Figure 1, our goal is to develop a microscale version of this platform. The advantage of this

mechanism is that the platform has full 6 degree-of-freedom (6-DOF) motion while the actuation is entirely planar and the joints are all flexure based, which are easy to manufacture in small scale. Our approach is to apply our 3 dimensional (3D) assembly technology [14] for the construction of this structure.

Our assembly technique is motivated by the probe-based approach initiated at NIST [15]. We extended the method to a multi-probe platform, and demonstrated the feasibility of an automated sub-millimeter part pick-up/rotation/insertion task with only vision feedback [14], [16]. A two-probe chopstick-like manipulation method has been proposed in [17]. Similar to human manipulation of chopsticks, the two probes form a narrow angle, and the sides of the probes are used to contact the parts. In contrast, we have an opposing probe arrangement which uses only the tip contact to allow easy part rotation between the tips [2], [6]. Most previous work in microassembly has used microgrippers or fixtures to grasp and manipulate the parts. Microgrippers are generally MEMS devices themselves or made out of another delicate material. The grippers require very tight alignment to grasp the part and prevent damage. This tolerance requirement is sometimes alleviated through the use of fixtures or compliant points on the parts [11] but this limits the design possibilities of the parts. Once the part has been grasped it is necessary to manipulate the part to achieve a spatial configuration. With a gripper it is necessary to move the entire fixture holding the gripper and often results in a very large assembly device [7], [18], [19]. With probe-based manipulation, it is possible to achieve a large range of configurations through simple prismatic motions. The current manipulation system is capable of spatial microassembly simply through prismatic probe motions and a rotating, translating die stage. The probes used are tungsten and have a $20\ \mu\text{m}$ diameter spherical tip.

The use of vision feedback, without a force sensor, is attractive, as force sensors at the microscale are very delicate and easily broken. We have found in our approach that maintaining the proper amount of squeeze force on the part is of critical importance. This step depends on several factors: direction of the probe squeezing motion, amplitude of the

This work is supported in part by the National Institute of Standards and Technology (NIST) under the Small Grant program and the Center for Automation Technologies and Systems (CATS) under a block grant from the New York State Office of Science, Technology, and Academic Research (NYSTAR).

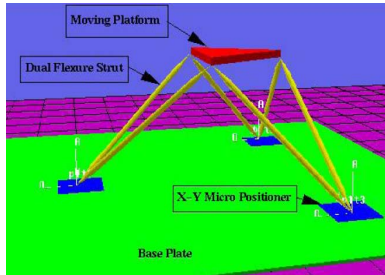


Fig. 1. Schematic of NIST 6-DOF platform positioner with planar actuators

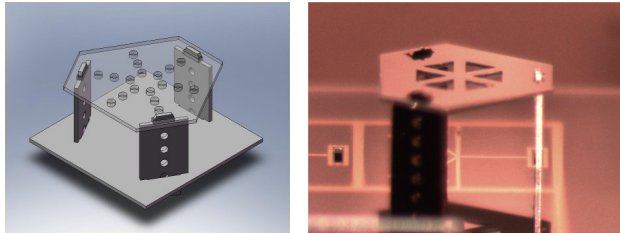


Fig. 2. Spatial microstructure CAD rendering and assembled device

probe squeezing motion, location of the contact in relation to part geometry, and the nature of the contact. To achieve reliable and robust multi-probe manipulation, we need to determine the best condition for the grasp, and then achieve this condition through robust vision feedback.

This paper reports on our initial result towards the assembly of a 6-DOF active microstructure by first constructing a passive spatial 3-legged microstructure. Figure 2 shows a Computer Aided Design (CAD) diagram of the microstructure to be assembled. This device is an example of a shape that may be useful in a future compliant, active device [13], [20]. The structure consists of three posts which measure $300\ \mu\text{m} \times 600\ \mu\text{m} \times 25\ \mu\text{m}$, and a hexagonal top piece that measures $600\ \mu\text{m} \times 600\ \mu\text{m} \times 25\ \mu\text{m}$. The parts were produced at the National Institute of Standards and Technology (NIST). This work builds on our previous work on a single part manipulation and insertion [14], [21]. We have applied this fully automated procedure to the insertion of the three legs. A top piece is then added to the structure using teleoperation.

II. EXPERIMENTAL TESTBED

Figure 3 shows the close-up view of the microassembly testbed. The major components of the systems are:

- The probes are mounted on two 3-DOF ThorLab NanoMax 600 positioners¹ in an opposed configuration. ($1.2\ \mu\text{m}$ step size, $2.4\ \mu\text{m}$ repeatability)

¹Certain commercial products and processes are identified in this paper to foster understanding. Such identification does not imply recommendation or endorsement by the National Institute of Standards and Technology, nor does it imply that the products and processes identified are necessarily the best available for the purpose.

- A 3-DOF die stage ($x-y-\theta$) consisting of a Newport CR4524 X-Y stage with EncoderDriver DC motor actuators and an OWIS Qmbh B-0308143X rotational stage with stepper motor. ($2\ \mu\text{m}$ linear accuracy, $< 0.017\ \text{mrad}$ rotation accuracy)
- Two 1.2 Megapixel C-mount microscope Firewire cameras with actuated zoom. These cameras are both Basler A631F cameras, with Edmund VZM450 zoom lenses. The Basler A631F Firewire camera has a maximum resolution of 1392×1040 pixels, with a large $1/2''$ progressive scan CCD array. When combined with the VZM450 lens, this provides a working resolution of between $3\ \mu\text{m}$ and $1.5\ \mu\text{m}$ per pixel depending on the zoom level. The lenses have been augmented with stepper motors to provide automated zoom capabilities. These lenses have a constant working distance over the entire zoom range. One camera is configured as an overhead camera, while another camera provides a side view approximately 20° off horizontal.
- Control electronics and MATLAB and Visual Basic based software interface

The system is designed around two actuated probe manipulators operating over a silicon die containing the device being assembled. The two manipulators are sharp-tipped probes ($20\ \mu\text{m}$ diameter) designed to manipulate small silicon parts. The probes are mounted on two 3-DOF stepper translational stages with about $1.2\ \mu\text{m}$ positional accuracy. The die itself is mounted on a 3-DOF (planar translation and rotation) stage mounted between the two probe stages. The die stage allows the die to be moved into and out of the relatively limited work space of the probes – the range of motion in any direction is only approximately $4\ \text{mm}$. With the combination of the motion of the probes and the motion of the die, manipulation can take place at any location on the $10\ \text{mm} \times 10\ \text{mm}$ die. The kinematic relationship between the various components in the system is determined through an automated vision based calibration procedure [14].

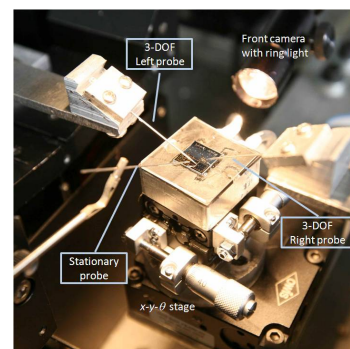


Fig. 3. Close-up View of the Microassembly Experimental Testbed

III. MULTI-PROBE MANIPULATION

The assembly process involves two tasks:

1. Leg pick up, rotation, and insertion
2. Insertion of platform into top of the legs

The first task is performed autonomously with minimal user supervision. The second task is performed by teleoperation at the present. This section presents the autonomous leg manipulation strategy using multiple-camera vision feedback.

The top camera only provides the x - y information of the probe tip and the part to be manipulated. The z -axis information requires the side camera. As a result, our strategy is to decouple the vision guided motion into x - y plane motion and z direction motion. Note that due to the light weight of the part (less than 1 μ N) and the low speed operation, only the kinematics need be considered. The post insertion is based on our previous work [14].

The leg manipulation task is decomposed into the following steps:

- 1) *Probe Positioning in x - y* : Move the probes in the x - y plane until they are next to the specified grasp point (in the x - y plane, about 5 μ m away from the part edge).
- 2) *Probe Positioning in z* : Move the probes in the z direction using the reflection of the probe (side camera alone does not provide high enough resolution), until they are just above the die stage (about 5 μ m, the part itself is 25 μ m).
- 3) *Grasping*: Move the probes together toward the edge until a firm grasp is established. The threshold of a secure grasp has been experimentally determined to be combined x direction error of 10 μ m.
- 4) *Part Lifting*: Coordinate both probes to maintain x direction separation and move vertically up towards the passive probe.
- 5) *Part Rotation*: Coordinate both probes to move the part until it presses against the passive probe while maintaining the grasp. The probes move in a direction perpendicular to the part surface and towards the passive probe, causing the part to rotate about the axis between the probes.
- 6) *Part Insertion*: The die stage positions the hole underneath the part, and the probes move the part into the hole while continuing to maintain grasp.
- 7) *Part Release*: The probes move quickly away from the part to release contact.

In the first step, only the top camera image feedback is needed for the positioning. In the second step, only the side camera is used. Therefore, the 3D multiple-camera vision calibration and image feedback is needed. Repeatability of the post insertion procedure is generally good, with most failures caused by the vision system being distracted by imperfections on the die and lighting issues. Currently the least repeatable steps are grasping and insertion. Grasping is around 70 % successful and can be easily repeated if it fails initially. Insertion has not been attempted a large number of times and

most failures are due to the vision system being distracted by noise. With some limited assistance the insertion success rate is around 80 %. The third probe rotation process is nearly always successful.

Assembling the top part was accomplished through telerobotic operation after all three of the posts had been assembled. The assembly process is simply to grasp the part, move it into position, align, and place on top of the posts. The part is normally moved with synchronized probe motions with slight differential movements to align at the end. This process was done manually to demonstrate the feasibility of the process. Repeatability of this process is low at the moment due to the human operator attempting to directly estimate relative position and orientation from the two views.

The procedure presented is highly experimental and is run at a very slow rate. The post insertion procedure for centering, grasping, flipping, and inserting takes between 8 min to 10 min per post. The top placement for this particular experiment took 17 min. The overall experiment lasted 3 h including setup. This time is far longer than a final commercial device would require to assemble the parts. The grasp dynamics are very fast and could potentially move the part at a higher velocity. With faster cameras and stages the assembly time in a commercial application could potentially be in the ten minute range, but this is very difficult to predict until faster systems are tested.

Because of the relatively early stage of this research, large tolerances were used for the slots to ease assembly. While this makes insertion simpler, it also can cause the posts to tilt to the side before assembly (See Figure 11 (f)). It was necessary to manually "poke" the posts vertical before placing the top piece. While this step is necessary for the experiment described, it may not be necessary in the future as tolerances are improved or the parts are glued in place immediately after insertion.

Grasping is a particularly interesting part of the two probe manipulation strategy. No force sensor is used due to their fragility. Instead, the deformation of the probe and part, as measured by the positioning error, is used for the threshold of a stable grasp. This is similar to image-based force sensing in [6]. If the probes are perfectly aligned, then this is a one-dimensional problem as shown in Figure 4. Assuming the undeformed spring length and the mass of the part are negligible, the part position x is given by the force balance:

$$k(x - \frac{\ell}{2} - x_1) + k(x + \frac{\ell}{2} - x_2) = 0 \quad (1)$$

where k is the spring constant, x is the center of the part, ℓ is the width of the part, and (x_1, x_2) are the contact locations for the two probes. Due to the quasi-static nature of the problem, we use a simple proportional kinematic control law to achieve the desired squeeze force:

$$\Delta x_1 = -k_p(x_1 - (x - \frac{\ell}{2}) - \delta) \quad (2)$$

$$\Delta x_2 = -k_p(x_2 - (x + \frac{\ell}{2}) + \delta) \quad (3)$$

where the target deformation, δ , needs to be carefully chosen through repeated experimentation. If it is chosen too low, the part cannot be lifted; if it is chosen too high, the part flies off. Our threshold of 10 μm corresponds to 1 mN to 3 mN of grasping force based on the modulus of the silicon part. Note that if the two probes are synchronized, then from (1), there will be no net motion. If there is a time delay between the two probe controllers, the feedback gain k_p needs to be chosen small enough to avoid oscillation.

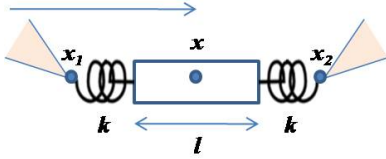


Fig. 4. Both probes aligned and squeezing the part

With the properly chosen deformation value (i.e., grasping force), the part/probe contact is essentially rigid, i.e., the contact can support full force and torque, provided that the values are not too large. The light weight parts in this application are less than 1 μN . In Section IV, the amount of contact force due to contact adhesion (van der Waals and capillary forces) is estimated to be about 50 μN . Therefore, the rigid contact assumption, in the absence of other external forces is a reasonable one. In Figure 5, the part is supported by a single probe (this is achieved by first grasping the part using both probes, and then removing one of them), further demonstrating the rigid contact at the probe/part contact. In this case, only the contact adhesion force is present to counteract the small inertial force of the part.

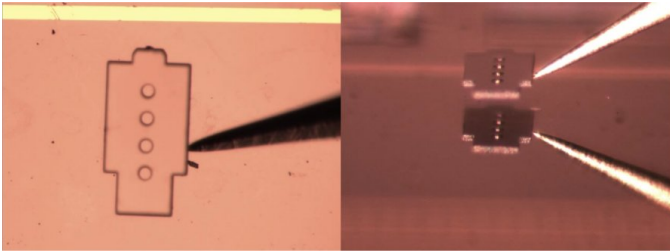


Fig. 5. Part supported by a single probe

Due to the positioning accuracy (around 1.2 μm) and image pixel resolution (between 1.5 μm and 3 μm , depending on the zoom level), there may be a slight misalignment of the probe in the y direction as shown in Figure 6. In this case, a moment about the vertical axis will be generated. Indeed, in our experiments, we have observed that the parts will sometimes rotate by a small angle. What prevents the part from continuing to rotate beyond this angle? Assuming

negligible inertia, the equation of motion is given by:

$$d_r \dot{\theta} + \left[k(x - \frac{\ell}{2} - x_1) - k(x + \frac{\ell}{2} - x_2) \right] h + \tau(\theta) = 0 \quad (4)$$

where h is the amount of misalignment, and τ is the additional z torque that we shall discuss below. We hypothesize that there are two mechanisms that prevent large angle part rotation. When the probes start to squeeze the part, the part will start to rotate. The indentation of the probe into the part will cause a reaction force in the y direction which will generate a z torque countering the moment due to the misaligned squeeze forces. There is also the adhesion force along the y direction that could also generate a z torque. Determining the precise mechanism would require further experimentation. As an order of magnitude calculation, the torque due to misalignment is $f_s h$ where f_s is the squeeze force $2k\delta$ and the counter torque due to adhesion force is $2f_a \ell$ where f_a is the contact adhesion force. To prevent undesired rotation, we would require

$$f_s < \frac{2f_a \ell}{h}. \quad (5)$$

Using representative values, $f_s=1$ mN and $f_a=50$ μN , we would require $\frac{\ell}{h} > 100$. For our part, $\ell=300$ μm , so the misalignment should not exceed 3 μm , which is well within the capability of our vision and positioning system. A similar analysis may be performed in the z misalignment, which should also be limited to about 3 μm .

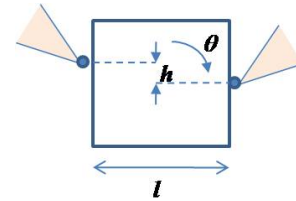


Fig. 6. Probe Misalignment in the y and z Directions

Another phenomenon that was observed is that the two probes are not perfectly synchronized in lifting and manipulating the part. This would result in a rotation about the y axis as shown in Figure 7. If the maximum delay is T and the probe motion velocity is v_z , resulting in the z direction misalignment of $v_z T$. The squeeze force f_s would then cause a moment about the y direction with magnitude $f_s v_z T$. Again, the adhesion force f_a would provide the counter-moment, $2f_a \ell$. This then translates to a limit to the maximum speed:

$$v_z < \frac{2f_a \ell}{f_s T}. \quad (6)$$

Using the representative values as before, and assume maximum of 5 ms delay, the maximum speed is 6 mm/s.

For the part rotation, the external force due to the pressing against the passive probe should be large enough to overcome the adhesion force so the contacts now become point contacts

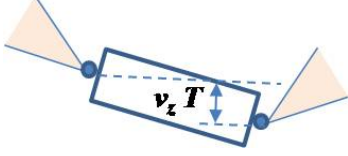


Fig. 7. Rotation due to Controller Delay between Probes

with friction (i.e., spherical joints). The motion of the part should be coordinated to ensure it is perpendicular to the part and towards the passive probe. We have implemented this by pre-scripting the motion, but it may be performed using vision feedback as well, to afford an additional level of robustness.

IV. CONTACT ADHESION

The contact between the probes and part may be considered as a spherical tungsten body in contact with a planar silicon body. A simple Hertzian contact model suggests that the tungsten sphere will deform at contact to produce a flat spot [22]. This flat area of contact provides the friction to prevent motion in the absence of large external force and moments. The contact radius between the sphere and plate is given by

$$a = \sqrt[3]{\frac{3Ft_1}{t_2}} \quad (7)$$

$$t_1 = \left(\frac{1 - \nu_1}{E_1} \right) + \left(\frac{1 - \nu_2}{E_2} \right) \quad (8)$$

$$t_2 = 8 \left(\frac{1}{d_1} \right) \quad (9)$$

where E_1 and E_2 are the Young's moduli of the probe and part, ν_1 and ν_2 are the Poisson ratios of the part and probe, d_1 is the diameter of the sphere, and F is the applied normal force. We have estimated the force between the probe and part to be 1 mN. Based on the parameters $E_1 = 400$ GPa, $E_2 = 100$ GPa, $\nu_1 = 0.22$, $\nu_2 = 0.28$, $d_1 = 20$ μm , and $F = 1$ mN, the resulting contact radius $a = 418.2$ nm.

At the micro scale, significant adhesion can occur between the part and probe [23]. The adhesion is created by van der Waals, capillary, and Coulomb forces. It is assumed the Coulomb forces do not play a significant role due to the conductivity of the probes. The van der Waals force consists of the force caused by the contact between the sphere and plate, and also additional contact due to deformation [24]. For the sphere-plate contact, we have

$$F_{vdw} = \frac{hr}{8\pi z^2} \quad (10)$$

With the van der Waals constant $h = 7$ eV, van der Waals distance $z = 0.4$ nm, and the tip radius $r = 10$ μm the result is $F_{vdw} = 2.8$ μN . When the flat contact has been formed due to deformation, the additional force is estimated as

$$F_{vdw,def} = \frac{ha^2}{8\pi^2 z^3} \quad (11)$$

where a is the contact radius from (9). With the initial 1 mN force, this works out to 38.82 μN of extra van der Waals force. The high level of extra adhesion generated requires a sizable initial deformation, and therefore a significant pressure applied to the part. This means that simply contacting the part with a light touch will not create a strong adhesion force. Force must first be applied at a relatively high level in order to create stiction.

Capillary attraction also provides adhesion between the part and probe. In a normal humid environment there is a thin layer of water that causes capillary attraction on most surfaces. The capillary force between a probe and part can be estimated as [25]

$$F_{cap} \approx 4\pi r \sigma_s \quad (12)$$

With a probe radius $r = 10$ μm and the surface energy of water $\sigma_s = 0.073$ N/m, the estimated capillary force is $F_{cap} = 9.174$ μN .

V. VISION FEEDBACK

The assembly process described above uses vision feedback to locate the probes, die, and parts, and to position and move them to desired locations. Joint position feedback alone is not sufficient to achieve the required accuracy.

Multiple-camera vision is implemented through the use of two cameras. The overhead camera provides a top-down view of the workspace. Its image plane is parallel to the die surface. The second camera is a perspective camera providing a front view. This camera is rotated about the x -axis 70° to provide a high angle view of the workspace. This angle was selected to provide a good measurement of the height information while still having the die surface in view. This configuration is similar to other microassembly workcells [7], [26].

The first step in system operation is calibrating the cameras. The intrinsic camera parameters are predetermined, so we only calculate the extrinsic position and orientation of the cameras. Figure 8 shows the reference grid used for calibration in the top and side views. The top camera is assumed to be telecentric and perfectly aligned to the die plane. Over the height of 500 μm for the system workspace this is valid to within approximately 2 μm . The side camera is calibrated using a standard pinhole camera model [27]. The focal length is predetermined, and is long enough that the side camera is also effectively telecentric. From the image it is clear that approximately 6 horizontal grid lines are in focus in the front view camera. This corresponds to an area approximately 500 $\mu\text{m} \times 500$ $\mu\text{m} \times 2000$ μm of 3D calibrated workspace.

The cameras are configured with motorized zoom and focus capabilities to allow for high resolution during grasp and part insertion operations. The height of the probes must be accurate enough to hit near the center of the thin edge of the part being grasped, which measures only 25 μm . To achieve this level of accuracy in height it is necessary to use the reflection of the probe on the surface. Figure 9 shows a high zoom image of the probe next to the edge of the part. This

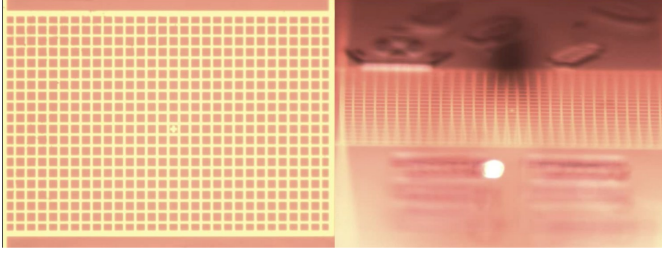


Fig. 8. Camera calibration pattern from top and side views

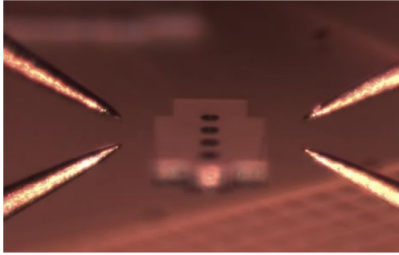


Fig. 9. Reflection of probes visible at high zoom. The top two probes are real, while the bottom two are near perfect reflections.

approach is a far more accurate measurement of the height than the pure stereo vision.

The other use for high zoom is visual force sensing during the grasp. It is possible to detect the actual position of the probe and compare it to the commanded position of the actuators [6]. This provides a sufficiently accurate estimate of the force to generate a repeatable robust grasp. Without this force information generating a grasp is nearly impossible.

The high zoom allows for resolutions of around 1.25 μm per pixel, but a limited depth of field in both cameras. For this reason it is challenging to calibrate a multi-camera vision model for this configuration. Instead, the two cameras are used independently with relative measurement operations rather than attempting absolute position localization in the world frame.

The different features in the workspace require different lighting conditions in order to be extracted by computer vision algorithms. The overhead microscope is equipped with a coaxial illumination and a ring light. The coaxial illuminator is used to detect the gold reference marks on the die, the probes, and the slots for insertion. Due to the parts being made out of the same material as the die, they are not directly visible with this illumination. The ring light illumination highlights the edge of the parts and is used for part detection. Figure 10 shows the same view with the two different illumination sources. The front camera is equipped with a separate ring light.

VI. EXPERIMENTAL RESULTS

Figure 11 shows snapshots of different points in the assembly of the structure. The assembly starts at (a) with the parts lying in the pickup area. Next, a part is centered and the

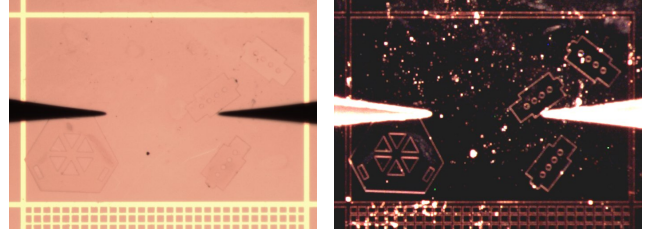


Fig. 10. Parts, probe, and die illuminated with coaxial (left) and ring (right) light sources

zoom is increased. A part grasp is initiated by pressing the probe against either side of the part as shown in (b), until the desired deformation (squeeze force) is achieved. The part is slightly lifted off the surface (c) by coordinating the motion of both probes. The part is next pressed against the third passive probe to generate the out-of-plane rotation. Panel (d) shows the part before the rotation; and (e) after. Panel (f) shows the three posts after insertion into the reception slots. Because of the loose tolerances of the slots the parts do not sit straight. It is necessary to "poke" them vertical before the top piece can be installed. Panel (g) shows the posts in their vertical configurations and the top piece being held over the posts. (h) shows the final assembled structure from the front camera, and (i) shows the structure from the overhead camera.

The structure was assembled using a combination of autonomous and telerobotic assembly. The three post grasp, rotation, and insertion sequences are based on the automated sequence. The post alignment and top placement was accomplished through teleoperation. Automatic implementation of this step is completely feasible. We are developing a general automated microassembly planner with this structure as the first test case.

VII. CONCLUSION

This paper describes a spatial microstructure that has been assembled using sharp-tip probes and computer vision through automatic and telerobotic operation without the need for fixtures, specialized grasp points, or snap-fasteners. The flexibility of the two-probe grasp is demonstrated by manipulating two different types of parts with no change to the grasp mechanics. The structure demonstrated is intended to represent the general configuration of a compliant micromechanism. Future designs will use the same assembly procedure with parts that contain compliant elements. The process will be completely automated with the use of an automated planner and a generalized grasp controller. The development of the planner will require a simulation that includes the unique microscale effects presented. Finally, different materials other than silicon will be investigated to provide more functional micromechanisms.

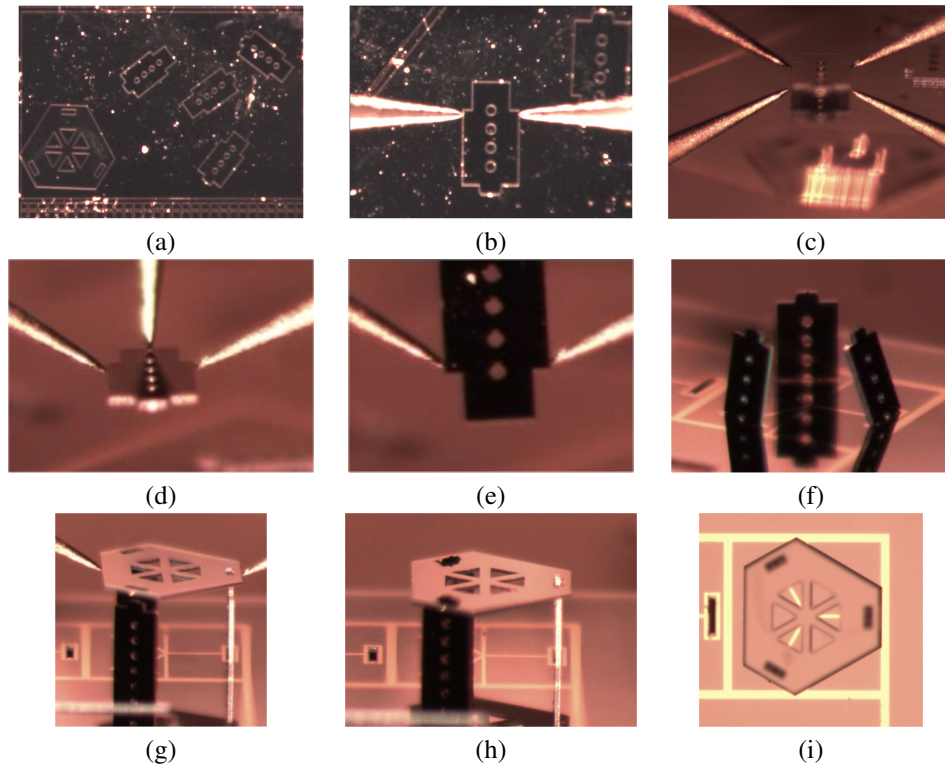


Fig. 11. Microstructure Assembly Snapshots

REFERENCES

- [1] W. Zesch and R. S. Fearing, "Alignment of microparts using force controlled pushing," in *SPIE Conference on Microrobotics and Microassembly*, vol. 3834, Boston, MA, 1998, pp. 195–202.
- [2] E. Shimada, J. Thompson, J. Yan, R. Wood, and R. Fearing, "Prototyping millirobots using dextrous microassembly and folding," in *ASME Symposium on Microrobotics*, 2000.
- [3] M. Moll, K. Goldberg, M. Erdmann, and R. Fearing, "Orienting micro-scale parts with squeeze and roll primitives," in *IEEE International Conference on Robotics and Automation*, Washington, DC, May 2002, pp. 1931 – 1936 vol.2.
- [4] J. Thompson and R. Fearing, "Automating microassembly with orthotweezers and force sensing," in *IEEE/RSJ International Conference on Intelligent Robots and Systems*, vol. 3, 2001.
- [5] N. Dechev, W. L. Cleghorn, and J. K. Mills, "Micro-assembly of micro-electromechanical components into 3D MEMS," *Canadian Journal of Computer and Electrical Engineering*, vol. 27, no. 1, pp. 7–15, Jan 2002.
- [6] A. Ferreira, C. Cassier, and S. Hirai, "Automatic microassembly system assisted by vision servoing and virtual reality," *IEEE/ASME Transactions on Mechatronics*, vol. 9, no. 2, pp. 321–333, June 2004.
- [7] B. N. G. Yang, J.A. Gaines, "Optomechatronic design of microassembly systems for manufacturing hybrid microsystems," in *IEEE Transactions on Industrial Electronics*, 2005, pp. 1013–1023.
- [8] D. Cappelleri, J. Fink, B. Mukundakrishnan, V. Kumar, and J. Trinkle, "Designing open-loop plans for planar micro-manipulation," in *IEEE Int. Conf. on Robotics and Automation, Orlando, FL*, 2006.
- [9] J. Fang and K. Böhringer, "Wafer-level packaging based on uniquely orienting self-assembly The DUE-SPASS Processes," *Journal Of Microelectromechanical Systems*, vol. 15, no. 3, pp. 531–540, 2006.
- [10] J. Abbot, Z. Nagy, F. Beyeler, and B. Nelson, "Robotics in the small," *IEEE Robotics & Automation Magazine*, vol. 14, no. 2, pp. 92–103, 2007.
- [11] D. Popa, W. Lee, R. Murthy, A. Das, and H. Stephanou, "High yield automated mems assembly," 2007, pp. 1099–1104.
- [12] A. Das, J. Sin, D. Popa, and H. Stephanou, "On the precision alignment and hybrid assembly aspects in manufacturing of a microspectrometer," in *IEEE Conference on Automation Science and Technology*, Washington, DC, August 2008.
- [13] N. G. Dagalakis and E. Amatucci, "Kinematic modeling of a 6 degree of freedom tri-stage micro-positioner," in *Proceedings of the ASPE Annual Meeting*, Crystal City, VA, 2001, pp. 200–203.
- [14] J. D. Wason, W. T. Gressick, J. T.-Y. Wen, J. J. Gorman, and N. G. Dagalakis, "Multi-probe micro-assembly," in *Third Annual IEEE Conference on Automation Science and Engineering*, Scottsdale, AZ, 2007.
- [15] J. J. Gorman and N. G. Dagalakis, "Probe-based micro-scale manipulation and assembly using force feedback," in *International Conference on Robotics and Remote Systems for Hazardous Environments*, Salt Lake City, UT, 2006, pp. 621–628.
- [16] J. Wason, "Multiprobe microassembly," Master's thesis, Rensselaer Polytechnic Institute, Troy, NY, 2007.
- [17] T. Tanikawa and T. Arai, "Development of a micro-manipulation system having a two-fingered micro-hand," *IEEE Transactions on Robotics and Automation*, no. 1, Feb. 1999.
- [18] N. Dechev, L. Ren, W. Liu, W. Leghorn, and J. Millis, "Development of a 6 degree of freedom robotic micromanipulator for use in 3d mems microassembly," in *IEEE International Conference on Robotics and Automation*, 2006, pp. 281–288.
- [19] N. Dechev, M. Basha, S. Chaudhuri, and S. Safavi-Naeini, "Microassembly of 3d micromirrors as building elements for optical mems switching," in *Proceedings of SPIE*, vol. 6376. SPIE, 2006, p. 63760C.
- [20] N. G. Dagalakis and E. G. Amatucci, "Six-degree of freedom micropositioner," U.S. Patent 6,484,602 B1, 2002.
- [21] J. D. Wason, W. T. Gressick, J. T.-Y. Wen, J. J. Gorman, and N. G. Dagalakis, "Multiprobe microassembly experimental testbed," in *International Conference on Micromanufacturing*, Pittsburg, PA, 2008.
- [22] J. Collins, *Mechanical Design of Machine Elements and Machines*. John Wiley & Sons, 2003.
- [23] R. Fearing, "Survey of sticking effects for micro parts handling," in

IEEE/RSJ International Conference on Intelligent Robots and Systems, 1995.

- [24] R. Bowling, "A theoretical review of particle adhesion," in *Particles on Surfaces I: Detection, Adhesion and Removal*, K. Mittal, Ed. New York: Plenum Press, 1988, pp. 129–155.
- [25] D. B. Asay and S. H. Kim, "Effects of adsorbed water layer structure on adhesion force of silicon oxide nanoasperity contact in humid ambient," *Journal Of Chemical Physics*, vol. 124, 2006.
- [26] K. Yesin and B. Nelson, "Robust cad model based visual tracking for 3d microassembly using image space potentials," in *Robotics and Automation, 2004. Proceedings. ICRA '04. 2004 IEEE International Conference on*, vol. 2, May 2004, pp. 1868–1873 Vol.2.
- [27] R. Haralick and L. Shapiro, *Computer and Robot Vision*. Addison-Wesley, 1992, vol. 1.